PSFC/JA-05-46

Advances in measurement and modeling of the high-confinement-mode pedestal on the Alcator C-Mod tokamak

J.W. Hughes, B. LaBombard, D.A. Mossessian, A.E. Hubbard,
J. Terry, T. Biewer and the Alcator C-Mod Team

December 2005

Plasma Science and Fusion Center
Massachusetts Institute of Technology
Cambridge, Massachusetts 02139

Submitted for publication in *Physics of Plasmas*

This work was supported in part by the U.S. Department of Energy Contract No. DE-FC02-99ER54512. Reproduction, translation, publication, use and disposal, in whole or in part, by or for the United States government is permitted.

This page left intentionally blank.

Advances in measurement and modeling of the high-confinement-mode pedestal on the Alcator C-Mod tokamak

J.W. Hughes, B. LaBombard, D.A. Mossessian, A.E. Hubbard, J. Terry, T. Biewer and the Alcator C-Mod Team

Abstract

Edge transport barrier (ETB) studies on the Alcator C-Mod tokamak [Phys. Plasmas **1**, 1511, (1994)] investigate pedestal scalings and radial transport of plasma and neutrals. Pedestal profiles show trends with plasma operational parameters such as total current I_P. A ballooning-like I_P^2 dependence is seen in the pressure gradient, despite calculated stability to ideal ballooning modes. A similar scaling is seen in the near scrape-off-layer for both low-confinement (L-mode) and H-mode discharges, possibly due to electromagnetic fluid drift turbulence setting transport near the separatrix. Neutral density diagnosis allows examination of D^0 fueling in H-modes, yielding profiles of effective particle diffusivity in the ETB, which vary as I_P is changed. Edge neutral transport is studied using a 1D kinetic treatment. In both experiment and modeling, the C-Mod density pedestal exhibits a weakly increasing pedestal density and a nearly invariant density pedestal width as the D^0 source rate increases. Identical modeling performed on pedestal profiles typical of DIII-D [Nucl. Fusion **42**, 614, (2002)] reveal differences in pedestal scalings qualitatively similar to experimental results.

I. INTRODUCTION

A critical consideration for future burning plasma experiments is the plasma edge, as conditions there have been shown in both experiment [1] [2] [3] [4] and modeling [5] [6] to impact obtained core plasma transport and global confinement. In tokamaks the high-confinement mode (H-mode) [7] provides favorable levels of confinement through the development of an edge transport barrier (ETB) localized to the vicinity of the the last closed flux surface (LCFS). ETB profiles exhibit sharp gradients in temperature and density, forming a pedestal upon which the core profiles can build up. Plans for the International Thermonuclear Experimental Reactor [8] (ITER) anticipate H-mode, though at present modeling is insufficient to predict what values the pedestal ought to take on, or how wide the ETB region will be, given known operational parameters (*e.g.* plasma current I_P, toroidal field B_T, and input power P_{in}). Pedestal scaling laws are sought in experimental data on existing tokamaks [9] [10] [11] [12], and attempts have been made to extrapolate current pedestal results to ITER [13]. However, without accurate physics-based pedestal models to help explain experimental results, predictions will always lack certainty.

This paper discusses experimental work on the Alcator C-Mod tokamak [14] intended to refine understanding of the important transport mechanisms in the ETB. Empirical scaling studies are important to developing intuition about the important physics at play in setting the ETB characteristics. Scalings for the edge electron density and electron pressure gradient are discussed in Sec. II, indicating evidence of profile stiffness. H-mode density is also seen to be remarkably insensitive to changes in gas fueling. Section III follows with a description of an experiment designed to infer plasma transport coefficients in the pedestal with high resolution. It is shown that plasma current (or safety factor q) has a substantial influence on effective particle diffusivity. The effect of fueling on the density pedestal at fixed plasma operational parameters is explored numerically in Sec. IV using a kinetic neutral transport model coupled with fixed plasma transport; qualitative agreement is obtained with experiment. Finally, Sec. V discusses further experimental work on the sensitivity of H-mode density to agressive gas puffing.

II. EMPIRICAL PEDESTAL SCALINGS

Experimental studies of the ETB on Alcator C-Mod have been facilitated by a number of diagnostics with millimeter-order spatial resolution. Chief among these is the edge Thomson scattering (ETS) system, which is used for routine collection of electron density (n_e) and temperature (T_e) profiles in a 3 cm region spanning the plasma LCFS. The nominal ETS radial resolution is 1.3 mm, when mapped along flux surfaces to the outboard midplane, allowing for the resolution of the short gradient scale lengths exhibited by these profiles upon transition to H-mode. By collecting sets of ETS pedestal data across a wide range of plasma operational parameters, several empirical scaling laws have been determined for specific pedestal parameters. To obtain pedestal parameters, profiles

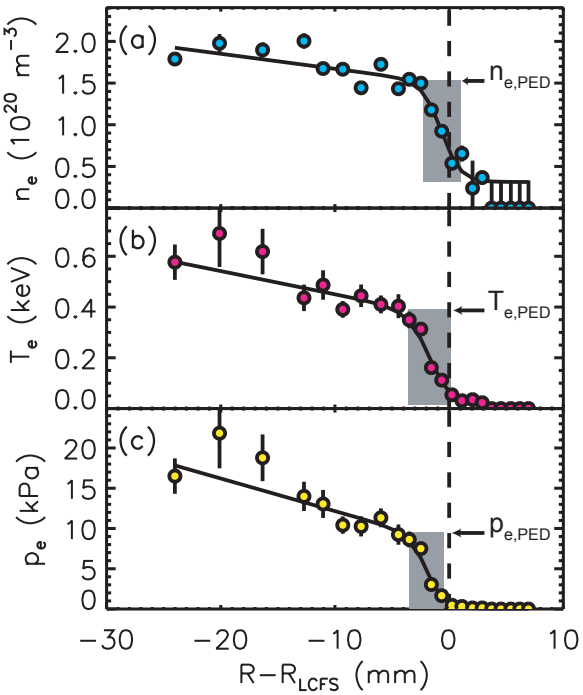

Figure 1: Simultaneous high-confinement mode (H-mode) profiles of (a) electron density n_e, (b) temperature T_e and (c) pressure p_e from edge Thomson scattering (ETS). The solid curves represent the results of fitting the H-mode profile data with the modified tanh function of Eq. (1). The gray boxes represent the extent of the pedestal region given by the four main fit parameters; the bottom and top borders of each box are given by b and $f_{\rm PED} = b + h$, while the left and right sides are $R_0 - \Delta/2$ and $R_0 + \Delta/2$. The vertical dashed line indicates the position of the last closed flux surface (LCFS).

of n_e, T_e and electron pressure $p_e = n_e T_e$ are fitted with a standard tanh-like function [15] defined on midplane major radius R:

$$f(R) = b + \frac{h}{2}\left[\tanh\left(\frac{R_0 - R}{\Delta/2}\right) + 1\right] + m(R_0 - R - \Delta/2)H(R_0 - R - \Delta/2) \qquad (1)$$

Here Δ, h and b are the pedestal width, height and base. The Heaviside function, $H(R_0 - R - \Delta/2)$, accounts for the finite radial slope, $-m$, that exists inside the pedestal region. Equation (1) has its maximum radial derivative at $R = R_0$: $|\nabla f|_0 = h/\Delta$. This notation will subsequently be used to denote the largest gradient of a given pedestal. Also, the subscript PED on a given variable will signify the value of that variable near the top of its pedestal (*e.g.*, $T_{e,\rm PED} = b_T + h_T$). Figure 1 shows typical profiles of T_e, n_e and p_e measured at a single time point in a C-Mod H-mode. The solid curves in the figure show the results of an error-weighted fitting of the tanh-like function of Eq. (1) to the measured profiles.

H-modes on C-Mod can usually be classified as either edge-localized-mode-free (ELM-free)

or enhanced D_α (EDA). The ELM-free regime represents a baseline H-mode with good plasma confinement, free of substantial edge fluctuations which drive transport of particles and energy into the scrape-off layer (SOL). Density and impurity build-up in the core plasma generally leads to a radiative collapse of the H-mode, making ELM-free H-modes inherently transient. The EDA regime [16] [17], on the other hand, has somewhat reduced energy confinement and a substantially enhanced level of particle recycling at the edge. Impurity accumulation is kept low, and an H-mode can be maintained steady state. The mechanism for this enhanced particle transport is a quasi-coherent mode (QCM), localized to the pedestal region [18] [19]. The QCM provides a continuous means of transport across the LCFS, in contrast to the intermittent bursts associated with ELMs [20]. Though operation at high input power can give a regime with small grassy ELMs [21], this regime of operation is not considered here. The predominance of the EDA H-mode regime and its steady state nature have made it amenable to characterization through pedestal scaling studies [22].

Operation at standard C-Mod shape ($\kappa \approx 1.7$, $\delta \approx 0.4$) results in a distribution of widths for the n_e, T_e pedestals in the range of 2–6 mm, with the mean Δ_{n_e} smaller than Δ_{T_e}. Even during a steady H-mode with fixed parameters, the fitted pedestal widths are seen to fluctuate considerably, giving a high level of profile variation consistent with the large edge fluctuations measured in EDA. Averaging pedestal data over steady portions of H-modes has helped to reduce the natural scatter in the data set. Under the typical operating conditions explored on C-Mod, the average pedestal width shows little systematic variation with operational parameters, contrary to a number of theoretical predictions [23]. A consequence of pedestal width invariance is that scalings for pedestal heights and gradients are similar in form.

A. Pressure gradient

Pressure pedestal scalings are of key interest, due to the strong correlation of this quantity with plasma confinement observed on a number of tokamaks [2] [4] [22]. One of the more prominent pedestal observations on C-Mod involves the scaling of the $p_{e,\mathrm{PED}}$ and $|\nabla p_e|_0$. As demonstrated in Ref. 22, plasma current I_P is the dominant variable in determining pedestal p_e, with a multiple linear regression on an EDA data set yielding

$$p_{e,\mathrm{PED}} \propto {I_P}^{2.0} \bar{n}_{e,L}^{-0.56} {P_{\mathrm{SOL}}}^{0.48}, \tag{2}$$

where $\bar{n}_{e,L}$ is the line-averaged target density in low-confinement mode (L-mode) and P_{SOL} is the net power transported into the SOL. A similar power law dependence is seen for $|\nabla p_e|_0$. While the I_P^2-dependence of pressure gradient is evocative of a pedestal limited by magnetohydrodynamic (MHD) ballooning modes, as noted on other tokamaks [4] [12] [24], modeling of edge stability in EDA discharges [25] has demonstrated stability to infinite-n ballooning modes given by ideal MHD, provided collisionally damped bootstrap current [26] is included in the calculation. In addition, when discharges were examined for instability to intermediate-n coupled peeling-ballooning modes

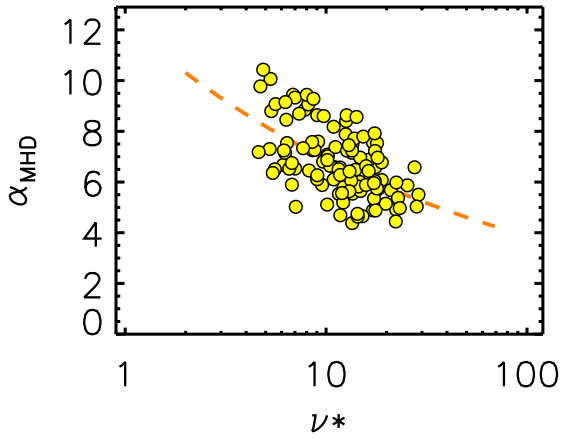

Figure 2: Normalized pressure gradient $\alpha_{\rm MHD}$ *vs.* collisionality $\nu^\star$ in the pedestals of EDA H-modes. The dashed curve represents a power law fit to the data: $\alpha_{\rm MHD} \propto \nu^{\star -1/4}$.

[27] [28] [29], EDA plasmas without grassy ELMs were found to be stable to these as well. Furthermore, the EDA discharges under study exhibit neither large nor small ELMs, which are the typical experimental manifestation of pedestal-limiting MHD activity. Rather, the plasma transport is a continuous process, apparently regulated by edge fluctuations. It is thus natural to ask whether this fluctuation-driven transport is responsible for setting the plasma gradients in the H-mode edge.

Such a mechanism has been sought in the near SOL of C-Mod, using profiles from scanning Langmuir probes [30] in ohmic discharges, typically without strong ETBs. Examination of probe data taken approximately 2 mm outside the LCFS has provided evidence for electromagnetic fluid drift turbulence [31] [32] setting the plasma transport state at this location. The study demonstrated experimentally both a local minimum in the pressure gradient scale length $L_{nT} = |nT/\nabla(nT)|$ and a functional dependence of normalized pressure gradient $\alpha_{\rm MHD} = 2\mu_0 q^2 R p'/B^2$ on a diamagnetic parameter α_d, which is an inverse collisionality reflecting the ratio of diamagnetic drift to resistive ballooning times [33] [34]. That is, *even in the absence of a strong ETB,* pressure gradient peaks locally and exhibits an I_P^2-dependence in the near SOL, with a constant of proportionality that depends on collisionality, thus mapping out a well-defined region in α_d-$\alpha_{\rm MHD}$ space. Ohmic H-mode data are few, but those that have been examined show a departure from this relationship, with higher values of $\alpha_{\rm MHD}$.

Since the near SOL marks the foot of the H-mode pedestal, it is reasonable to ask whether, in H-modes with no ELMy activity, similar physical mechanisms induce a stiffness in the edge poloidal beta gradient and give the observed $|\nabla p_e|_0 \propto I_P^2$ scaling of Eq. (2). Observing this scaling law and noting from Ref. 22 that $T_{e,\rm PED} \propto P_{\rm SOL}^{1/2}$, it is seen that lower edge collisionality (higher T_e, lower n_e) should allow for increased $\alpha_{\rm MHD} \propto \nabla p/I_P^2$. This is shown explicitly in Fig. 2 for the same data set used to produce the scaling law of Eq. (2). Here $\alpha_{\rm MHD}$ and plasma collisionality $\nu^\star$

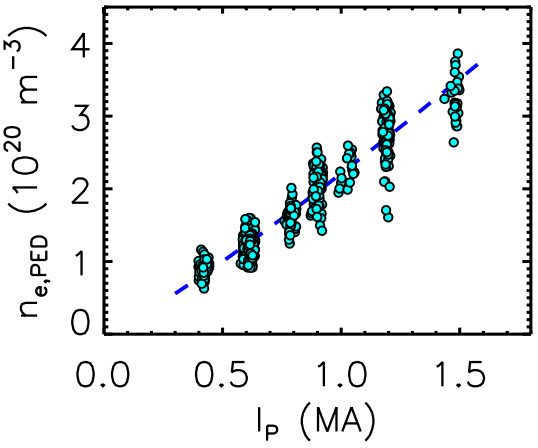

Figure 3: Density pedestal $n_{e,\mathrm{PED}}$ scales linearly with plasma current I_P across nearly a 4× variation. Data are from single ETS time points in H-modes during current flat top, with nearly constant stored energy $[W_P/(dW_P/dt) > 1\mathrm{s}]$.

are calculated using values for n_e, T_e and $|\nabla p_e|_0$ at the pedestal midpoint, and with q taken at the 95% flux surface (q_{95}). A weak trend of $\alpha_{\mathrm{MHD}} \propto \nu^{\star -1/4}$ is derived from the data, suggesting that collisionality plays a role in setting the normalized ∇p_e, just as in the aforementioned ohmic data. Interestingly, indications from prior pedestal characterization studies [22] are that, in H-mode, the threshold α_{MHD} for attaining the QCM and EDA H-modes is also a decreasing function of $\nu^\star$.

B. Density pedestal

Total plasma current also plays a dominant role in setting the n_e pedestal characteristics. $n_{e,\mathrm{PED}}$ scales linearly with I_P, while scaling either weakly or not at all with other plasma control variables such as magnetic field, input power and neutral fueling. This was first demonstrated for steady EDA H-modes with $0.6 < I_P[\mathrm{MA}] < 1.2$ and $4.5 < B_T[\mathrm{T}] < 6.0$ [22], but recent efforts to extend the range of parameters in pedestal scaling studies show that the $n_{e,\mathrm{PED}} \propto I_P$ scaling extends across both EDA and ELM-free regimes with currents from 0.4 to 1.5 MA. The trend is illustrated in Fig. 3, which includes points in an extended B_T range of 2.7–6.3 T. (Of note is that across this range in field there is no systematic B_T dependence, which indicates that the previously reported scaling [22] of $n_{e,\mathrm{PED}} \propto B_T^{-1/2}$ was overestimated, or was perhaps only present in the data set at higher B_T.) Robust dependence on a single plasma parameter that is irrelevant to neutral-plasma interactions suggests that the density pedestal is determined in large part by plasma transport mechanisms, and not solely by edge particle fueling. We nonetheless expect the neutral source to play a role in defining the density pedestal, and so correlations between pedestal parameters and fueling parameters are sought.

Density control on C-Mod is by means of a fast regulated gas valve with real time feedback

from interferometry, having a programmed target density $\bar{n}_{e,L}$ in the range of 1–2$\times 10^{20}$ m^{-3}. This system maintains a flat density trace in ohmic and L-mode shots. In H-mode the measured density generally exceeds the programmed density by a considerable margin, the gas puff ceases, and the plasma is fueled completely by recycling neutrals from the walls. The L-mode $\bar{n}_{e,L}$ does, however, provide a knob for adjusting the resulting pedestal density in H-mode at fixed I_P. Previous scalings studies [22] indicated that at fixed plasma parameters, the value of $n_{e,\mathrm{PED}}$ also depends on $\bar{n}_{e,L}^{0.4}$, despite the termination of active fueling upon H-mode formation. Because H-mode pedestal density is expected to be correlated with neutral flux, the result suggests that the L-mode target density is responsible for setting a persistent fueling boundary condition at the LCFS. The weakly positive scaling with $\bar{n}_{e,L}$ can be understood in terms of the initial fueling source on which the H-mode is allowed to draw. This scaling can be tested directly by fixing I_P, B_T and magnetic equilibrium shape for several discharges while varying the neutral source via L-mode density. Pedestal density data as a function of $\bar{n}_{e,L}$ are shown in Fig. 4a. Consistent with the scaling above, doubling the target density resulted in a 30–40% increase in $n_{e,\mathrm{PED}}$.

Based on simple 1D fluid modeling that invokes a radial flux balance between ions and neutrals, the density pedestal width is expected to scale as $\Delta_n \propto 1/n_{\mathrm{PED}}$, with gradient scaling as $|\nabla n_e| \propto n_{\mathrm{PED}}^2$ [35] [36]. Such scaling trends are indeed observed on the DIII-D tokamak [37], a device roughly 2.5 times the size of C-Mod that typically operates at less than one-third the usual C-Mod density. Employing active puffing and pumping of H-modes, a wide range of pedestal densities has been reported, with trends in width and gradient fit quite well by the simple fluid model. [35] As shown in Sec. V, puffing into typical C-Mod H-modes has little effect on $n_{e,\mathrm{PED}}$ or Δ_{n_e}. Furthermore, no evidence of these pedestal scalings is seen by scanning $\bar{n}_{e,L}$. By way of example, Fig. 4b shows no obvious dependence of width on pedestal density during the $\bar{n}_{e,L}$ scan at fixed I_P. If a trend exists, it is unseen due to both uncertainties in the measured pedestal parameters and the limited range in $n_{e,\mathrm{PED}}$.

Motivated in part by the above observations, an experiment was recently performed, aimed at examining in detail the changes in pedestal profiles, QCM behavior and transport of plasma and neutrals as current and density are varied. H-modes were induced using input ion cyclotron range of frequencies (ICRF) power at fixed shape, B_T and P_{in}, but varying the current among three nominal values: 0.46, 0.77 and 0.98 MA (giving $q_{95} \approx 9$, 5.5 and 4.2, respectively). Discharges at $q_{95} \approx 5.5$ demonstrated the ordinary EDA behavior, exhibiting a strong QCM and reaching a steady-state global density. At $q_{95} \approx 4.2$, the QCM became weaker, and density and impurity accumulation became an obstacle to achieving steady state H-mode. The high-q discharges displayed a QCM that was rather broad in frequency space and with a low overall amplitude; density in H-mode reached steady state, but the overall density increase above that in L-mode was marginal. Profiles measured with ETS clearly show the familiar trend of $n_{e,\mathrm{PED}}$ decreasing with lower I_P. Even when target density was varied by a factor of 2 at constant I_P little effect was seen on $n_{e,\mathrm{PED}}$. Figure 5 shows the trends observed in Δ_{n_e} and $|\nabla n_e|_0$ as a function of $n_{e,\mathrm{PED}}$, with clear clusters of data

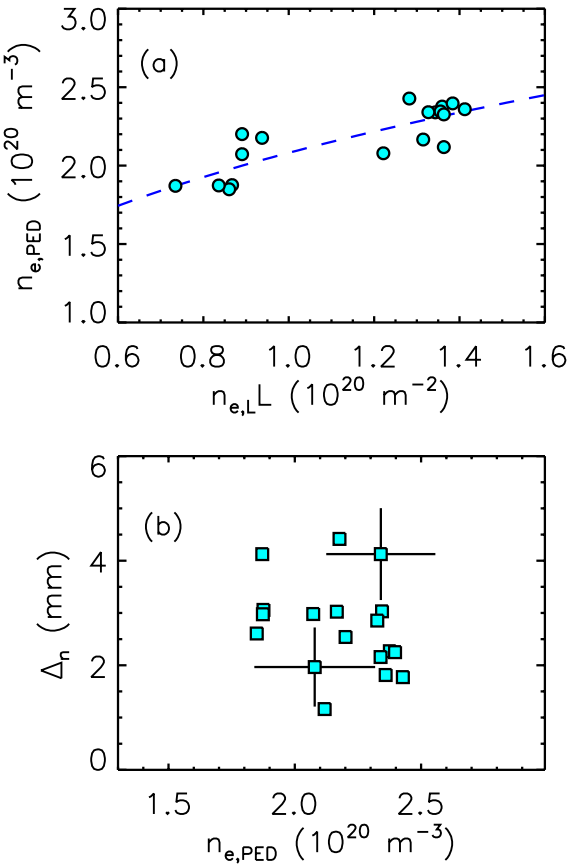

Figure 4: Results of a density scan in 0.8MA, 5.4T plasmas, with input power regulated such that $T_{e,\mathrm{PED}} \approx 300$ eV. (a) Density pedestal as a function of line-integrated target density $\bar{n}_{e,L} \times L$, along with a power law fit (dashed curve) to the data yielding $n_{e,\mathrm{PED}} \propto \bar{n}_{e,L}^{0.4}$. (b) Pedestal width in the same discharges *vs.* $n_{e,\mathrm{PED}}$. Typical error bars are plotted for two points. No significant variation in Δ_n is obtained.

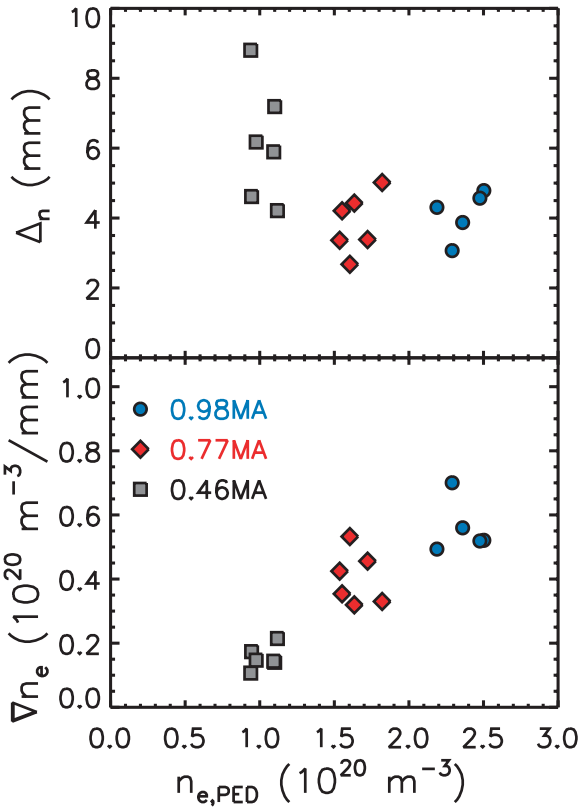

Figure 5: Pedestal trends in families of discharges at three distinct currents. (a) Density pedestal widths are in the usual range for the 0.77 and 0.98 MA discharges, but become much wider at $I_P = 0.46$ MA. (b) $|\nabla n_e|$ drops dramatically when going to the lowest current as well. These parameters are derived from modified tanh-fits to time-averaged ETS profiles.

appearing at the three I_P points. An obvious departure from nearly constant pedestal width behavior seen in earlier experiments is observed in Fig. 5a at low I_P. In this low-confinement H-mode, Δ_{n_e} takes on values from 4 to 10 mm at the midplane. Exceptionally small gradients are also exhibited (5b), no more than double the typical values of $|\nabla n_e|$ in L-mode.

Though the overall trends in Fig. 5 are suggestive of the simple scalings derived from the fluid model, inspection of the figure shows that, for a given I_P, there is no evidence of either $\Delta_{n_e} \propto 1/n_e$ or $\nabla n_e \propto n_e^2$, just as for the data shown in Fig. 4. Rather, the trend is indicative of a significant relaxation of the pedestal at low I_P, simultaneous with the correlation between I_P and $n_{e,\mathrm{PED}}$. As noted above, the QCM is a crucial component of the particle transport drive through the pedestal, and the amplitude and other characteristics of the mode are seen to change as I_P (or equivalently, q_{95}) is changed. This motivates us to examine the contribution of the intrinsic fluctuation-driven transport to the characteristic n_e profile shape. Experimental efforts in this direction is discussed below in in Sec. III. At the same time, as absolute pedestal density changes by large factors, characteristic neutral mean free paths change, and thus the feedback between plasma transport and fueling characteristics must be considered. This subject is considered in Sec. IV.

III. DIAGNOSIS OF PARTICLE TRANSPORT

Combined high resolution profiles from various edge diagnostics afford the opportunity for improved diagnosis of the particle transport in EDA H-mode pedestals. The experimental goal is to resolve the relative contributions of plasma transport and neutral penetration in determining how the plasma pedestal scales. Because the QCM so strongly drives particle transport through the pedestal, it is conceivable that plasma transport plays the dominant role in determining $n_{e,\mathrm{PED}}$ and Δ_{n_e}. The role of neutral fueling will be taken up in a later section.

After mapping to the midplane, ETS and probe data are used to construct radial n_e, T_e profiles extending from the core plasma into the far SOL. Composite profiles recorded during the I_P scan described in Sec. II are shown in Fig. 6a,b. Neutral density profiles at the edge are then determined by combining these data with measurements of background D_α from an outboard midplane gas puff imaging camera [38] operating at 60 fps and having approximately 2 mm resolution. Radial brightness profiles are determined from time-averaged camera data and Abel inverted to arrive at profiles of D_α emissivity, as in Fig. 6c. Unlike n_e and T_e, neutral emissivity can exhibit significant poloidal and toroidal variation. Because the tangential camera view is nearly horizontal, we ignore poloidal variation. We further assume that toroidal variation is small along the extent of the relevant viewing chords, since strongly localized sources of neutrals near the view are not anticipated under normal operation. This assumption has not been verified experimentally and poses a possible limitation to the analysis. Nonetheless, reasonable results follow. From n_e, T_e and the emissivity, the neutral density n_D (Fig. 6d) and ionization rate S_{ion} (Fig. 6e) are calculated using the Johnson-Hinnov collisional-radiative model [39]. One can see that in the 0.98 MA case, a peak

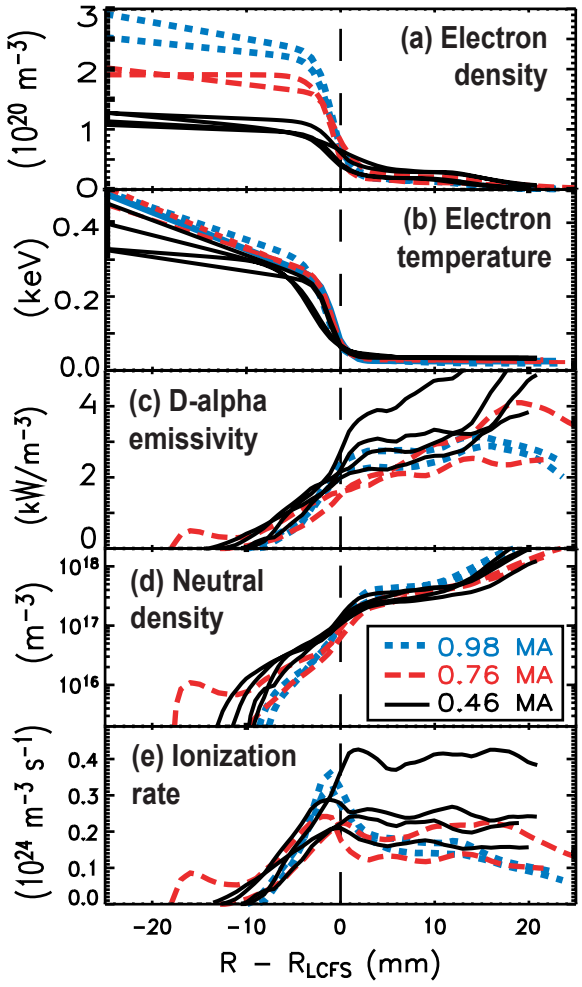

Figure 6: Using spatially resolved profiles of (a) n_e and (b) T_e from ETS and probes and (c) intrinsic D_α emissivity measured with a tangentially viewing camera, profiles of (d) neutral density and (e) ionization rate are determined for three families of discharges at distinct currents.

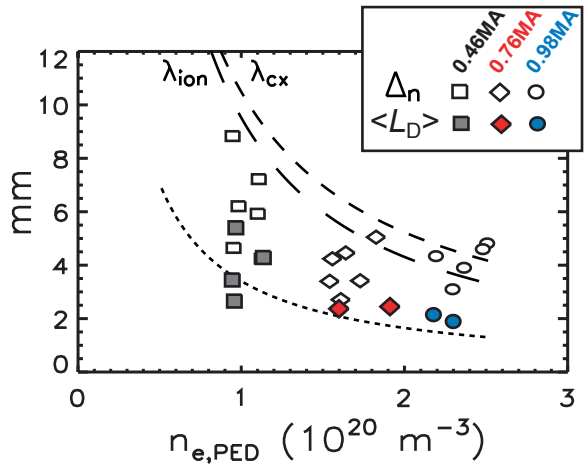

Figure 7: Direct comparison of average neutral gradient scale length $\langle L_D \rangle$ (filled symbols) with density pedestal width Δ_{n_e} (open symbols). The maximum values of Δ_{n_e} are comparable with estimations of ionization and charge exchange (CX) mean free path (MFP) $\lambda_{\rm ion}$, $\lambda_{\rm CX}$. Typically $\langle L_D \rangle$ is smaller than MFP estimations and Δ_{n_e}.

in $S_{\rm ion}$ occurs in the density pedestal. As current is lowered the relative distribution of ionization begins to shift from inside the LCFS to outside. The peak in $S_{\rm ion}$ disappears at smaller I_P, and at 0.46 MA, the SOL region is highly ionizing and a large source of D_α. The results are consistent with enhanced particle transport into the SOL at higher q, which generally results in a higher SOL n_e.

Of course, significant ionization occurs in the core plasma, and at $I_P = 0.46$ MA, the small pedestal density results in a longer average penetration length for neutrals, and considerably deeper penetration for the n_D profile (Fig. 6d). Local gradient scale lengths for both the n_e and n_D profiles tend to be less than simple estimates of neutral mean free path (MFP) based on ionization and charge exchange (CX) cross-sections, as shown in Fig. 7. Here the dashed curves represent $\lambda_{\rm ion} = v_D/n_e\langle\sigma v\rangle_{\rm ion}$ and $\lambda_{\rm CX} = v_D/n_e\langle\sigma v\rangle_{\rm CX}$ with the n_e and $\langle\sigma v\rangle$ evaluated for average values of n_e and T_e in the pedestal, and neutral velocity v_D determined by the thermal velocity of SOL neutrals with a temperature of 20 eV. These values of MFP are approximately the same as the maximum pedestal width obtained from the tanh-fits to the ETS and probe data. However, the average neutral gradient scale lengths $\langle L_D \rangle$ are much smaller than both pedestal width and estimated MFPs. This result indicates that simple estimates of the characteristic neutral penetration length, such as $\lambda_{\rm ion}$ and $(\lambda_{\rm ion}\lambda_{\rm CX})^{1/2}$, may not adequately model real n_D profiles in C-Mod H-modes. A possible source for the discrepancy is the choice of a fixed neutral velocity based on estimated SOL neutral temperature, which fails to account for spatial variation of the neutral distribution function, including energy transfer via CX and significant departures from a Maxwellian distribution. In the next section, a kinetic treatment that does account for the complete distribution function will be

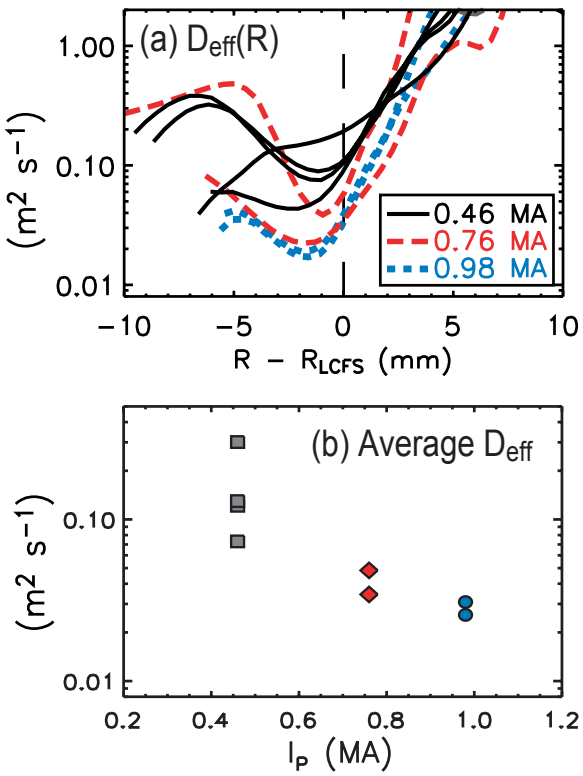

Figure 8: Effective diffusivity D_{eff} in the pedestal at varying I_P. (a) Spatially resolved profiles obtained using the density and ionization rate data in Fig. 6. (b) D_{eff} averaged over the extent of the pedestal region. There is a substantial drop in particle transport as I_P is increased from 0.46 MA to more typical C-Mod currents.

used to determine neutral penetration, showing qualitative agreement with this experimental result.

Based on the measurements shown in Fig. 6, it is possible to infer profiles of effective diffusivity D_{eff}, assuming transport according to $\Gamma_i = -D_{\text{eff}} \nabla n_i$ where Γ_i is radial ion flux and n_i is ion density. This is not meant to imply that the ion transport is purely diffusive in nature; rather, D_{eff} provides a useful metric for evaluating the level of both diffusive and convective transport. Assuming that local radial fluxes balance local ionization, S_{ion} can be integrated to yield the ion flux profile $\Gamma_i(R)$. This regime of "radial flux balance" is found to be present in C-Mod where the plasma is fueled by "main-chamber recycling" [40]. The diffusivity profiles, calculated from $D_{\text{eff}} = -\Gamma_i / \nabla n_e$, are shown in Fig. 8a. A well in D_{eff} is present in the pedestal region in all cases, and it is clearly seen to grow deeper as I_P is increased from 0.46 MA to more typical C-Mod currents. Inside the pedestal, values of D_{eff} appear to be in the range of 0.04–0.3 m^2/s, while closer to the LCFS, the minima are typically at 0.02–0.09 m^2/s. The width of the well is approximately 5 mm and has no obvious scaling with current. However, more radial structure could exist farther inside the core plasma, but be unnoticed, given the small values of measured D_α emissivity in this

region. In all cases the diffusivity rises to 1 m^2/s or higher just a few millimeters into the SOL. Beyond this point, radial plasma transport is known to exhibit bursty behavior, forming plasma "blobs" that are rapidly advected outward, leading to relatively flat average n_e profiles and high effective transport coefficients [32].

The trend of decreasing D_{eff} with increasing current is highlighted in Fig. 8b, where the diffusivity has been averaged over the pedestal region. Particle confinement at 0.46 MA is clearly quite low, nearly reaching L-mode levels. Given that the inferred D_{eff} well is similar in width to the pedestal extent and is not obviously correlated with analytical estimates of neutral penetration length, it is reasonable to suspect that Δ_{n_e} is determined by the extent of the region in which plasma transport is suppressed. If this is indeed the case, then a D_{eff} well of fixed width and variable magnitude should yield a pedestal of roughly fixed width and variable gradient. If so, then $n_{e,\text{PED}}$ should scale inversely with average D_{eff}. The implication is that increasing I_P raises the pedestal density simply by driving D_{eff} lower.

IV. MODELING

Ionization of neutrals at the tokamak edge fuels the plasma, and simple modeling of neutral fueling [36] tends to treat neutral species with a fluid analysis, employing ionization as a neutral particle sink. The ionization rate is given by $S_{\text{ion}} = n_D n_e \langle \sigma v \rangle_{\text{ion}}$, where the velocity-averaged cross section $\langle \sigma v \rangle_{\text{ion}}$ is a function of T_e only. Thus, neutral temperature T_D does not play a role in the ionization rate, and one need only assume a neutral fluid velocity v_D in determining λ_{ion}, as was done in the previous section. It is customary to take for v_D a value consistent with the expected thermal velocity of the neutral species as they pass into the plasma. This assumption, combined with reasonable assumptions for the plasma D_{eff} profile and LCFS boundary conditions, has been shown [35] [36] to give n_e pedestal profiles like those in experiment, and having the same width and gradient scalings (see Sec. II.B) demonstrated experimentally on DIII-D. Despite its successes, this simple fluid model does not incorporate momentum and energy exchange between ions and neutrals, processes which are expected to be important on C-Mod, due to both high n_i and large T_i gradients in the H-mode pedestal. One approach to incorporating these processes is simply to add momentum and energy balance to the existing neutral fluid model. However, this method might still neglect important corrections to the neutral distribution function that could only be determined using a fully kinetic treatment [41]. The kinetic approach is taken here; a discussion of more advanced fluid modeling and a comparison with kinetic results will be taken up in a future paper.

A *K*inetic *N*eutral *1-D* transport code (KN1D) was used to compute neutral distribution functions of both D_2 and D^0 in the tokamak edge, accounting for ionization, CX and elastic scattering on both ions and neutrals [42]. The computational grid is 1D in space along an axis x that is normal to the LCFS, with $x > 0$ corresponding to confined plasma and $x < 0$ being the SOL region. Key inputs to the code include background profiles of n_i (assumed equal to n_e), T_i and T_e. The

input gas pressure at the vessel wall serves as a knob for tuning the neutral source. The distribution functions for molecular and atomic species $f_{\mathrm{D}_2}(v,x)$, $f_{\mathrm{D}}(v,x)$ are evolved by self-consistently solving the Boltzmann equation

$$v_x \frac{\partial f}{\partial x} = \left[\frac{\partial f}{\partial t}\right]_{\mathrm{coll}} + S \tag{3}$$

for each species over multiple collision generations. Here $[\partial f/\partial t]_{\mathrm{coll}}$ accounts for the various collisions either species can experience, and S represents the net source. With the full distribution functions determined, it is straightforward to calculate n_D, T_D and v_D by taking the appropriate moments. Due to the large ion-neutral collision frequency and high ∇T_i present in modeled C-Mod pedestals, large gradients in T_D and v_D are found from KN1D, in contrast to simple fluid modeling. Departures from a Maxwellian velocity distribution are observed, though it is not yet certain whether these are significant enough to require kinetic corrections to the fluid moments.

KN1D contains no plasma physics, and so using the code to examine fueling in the pedestal requires some model for the plasma transport. We begin by assuming the neutral and ion fluxes balance ($\Gamma_D = -\Gamma_i$) and that the ion density n_i obeys Fick's Law, such that

$$\Gamma_D = -\Gamma_i = D_{\mathrm{eff}} \nabla n_i \tag{4}$$

An initial KN1D calculation using a starting set of model plasma profiles ($n_e = n_i$, $T_e = T_i$) yields a Γ_D profile, which allows computation of a D_{eff} profile from Eq. 4. Now we proceed under the premise that fixing all disharge operating parameters and adding a small perturbation to the neutral source does not significantly affect either the temperature pedestal or the diffusivity profile. KN1D is run with a slightly higher (lower) neutral density, leading to increased (decreased) Γ_D. Holding D_{eff} fixed, Eq. 4 determines a new n_i pedestal, which can then be used as input to the next KN1D computation. Each KN1D iteration assumes unchanged profiles of D_{eff} and $T_i = T_e$. Once the iterations converge, the fueling response of the n_i pedestal is determined.

Figure 9 shows the result when the neutral source perturbation technique is applied to experimentally determined plasma profiles from a 0.98MA discharge. In addition to the base case, neutral pressure scale factors F of 0.5, 0.75, 1.25 and 1.5 are tested. As fueling is increased, the modeled n_i profile increases and neutral penetration is significantly reduced (Fig. 9a–b). Pedestal width remains roughly fixed, while pedestal value grows slowly with neutral input, scaling roughly as $F^{1/2}$ and bearing a strong resemblance to the previously determined empirical scaling law for $n_{e,\mathrm{PED}}$ with $\bar{n}_{e,L}$. This trend is explicitly shown in Fig. 10 for the three I_P values considered in experiment. Figure 9c shows profiles of gradient scale length for both plasma (L_n) and neutrals (L_D), demonstrating $L_D < L_n$ throughout most of the pedestal region, as was seen in experiment. The figure also demonstrates a somewhat remarkable self-similarity among the resultant n_i profiles, at least within the LCFS. Constant gradient scale length L_n implies fixed pedestal width and ∇n scaling roughly with $n_{e,\mathrm{PED}}$. This contrasts with predictions of the simple fluid model for neutrals, but is in qualitative agreement with C-Mod experimental results. With increased fueling

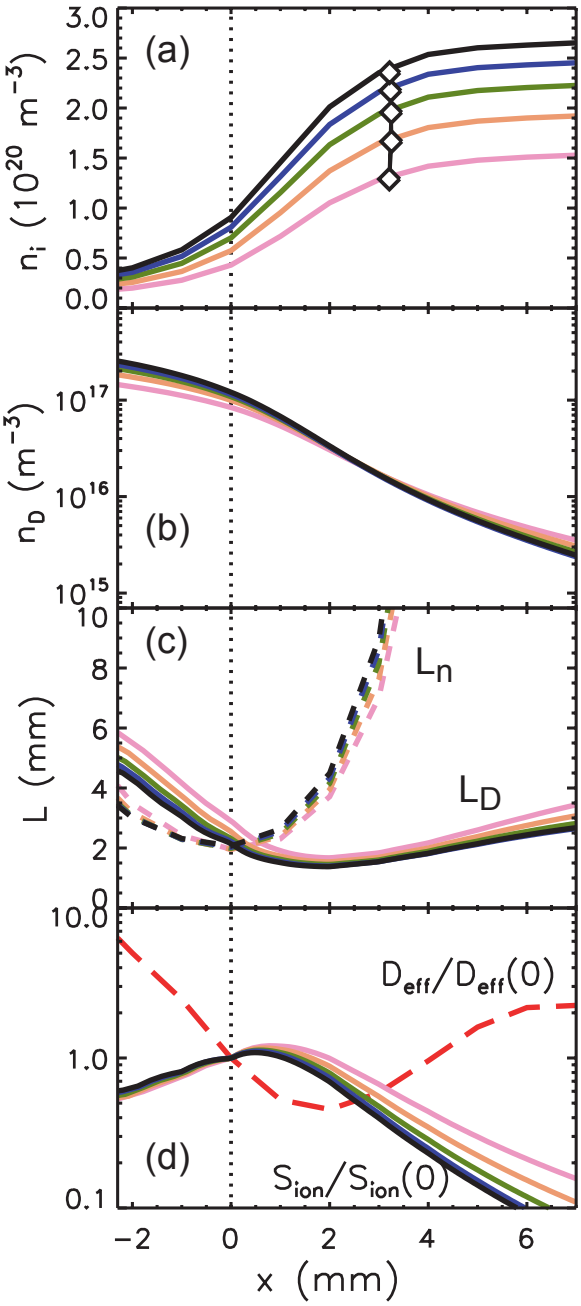

Figure 9: Example profiles from a simulation of fueling perturbation on a C-Mod density pedestal from a 0.98MA discharge, using a kinetic treatment for the neutral transport. (a) Computed ion density (n_i) pedestals show an overall rise with neutral source, with pedestal width changing little. Diamonds represent the top of the pedestal given by fiting the profiles with Eq. 1. (b) Resulting neutral density (n_D) profiles. (c) Local gradient scale lengths of n_i (dashed) and n_D (solid). (d) Profile shapes for the ionization rate $S_{\rm ion}$ (solid) and the $D_{\rm eff}$ (dashed) used to model the plasma transport.

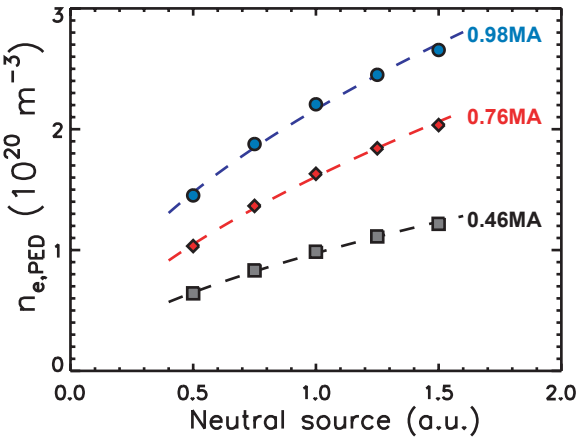

Figure 10: Computed density pedestal response to neutral source perturbations, at three distinct plasma currents. In each case $n_{e,\mathrm{PED}}$ scales roughly as the square root of the neutral source.

the ionization profile becomes narrower, and fueling appears to be increasingly localized to the foot of the pedestal (Fig. 9d). The high ionization rate in the outer portion of the inferred D_{eff} well appears to lead to density "pile-up" and a largely self-screening pedestal.

It should be noted that this analysis is only expected to be valid for small neutral source perturbations. Operationally, large increases in the neutral source lead to T_{PED} depression, and the resulting increase in collisionality has the potential to change fundamentally the edge flux-gradient relationships, as touched on in Sec. II. Sufficient T or ∇p suppression through excess fueling can lead to a Type III ELMy regime [20], or to no H-mode at all, and in extreme cases can lead to a Greenwald density limit disruption [43].

Performing this analysis on profiles more typical of the DIII-D tokamak yields slightly different results, as shown in Fig. 11. In this case a model pedestal of approximately 2×10^{19} m^{-3} is chosen, with $\Delta_n \approx 20$ mm. Again, the density rises with increased neutral source (Fig. 11a); however, in this case, the pedestal becomes narrower as n_{PED} increases. Moreover, Fig. 11c shows that the plasma gradient scale length decreases at higher densities. Thus the n_i profile is not stiff and its response to neutral perturbation is qualitatively consistent with experimental DIII-D results. At such low plasma density, neutral density falls off less sharply than on C-Mod (Fig. 11b,c), and neutrals penetrate a greater distance, relative to the ETB width, leading to a flatter and more invariant S_{ion} distribution (Fig. 11d) as density pile-up at the pedestal foot is reduced. The results point to a significantly reduced level of neutral screening at low plasma densities, and to trends predicted by the simple fluid model for neutral transport. At the highest densities tested, the n_i profile appears to take on a nearly constant gradient scale length, just as is the case on C-Mod. Referring to the L_n curves in Fig. 11c, it seems that this effect may already be important for $n_{\mathrm{PED}} \gtrsim 2 \times 10^{19}$ m^{-3}.

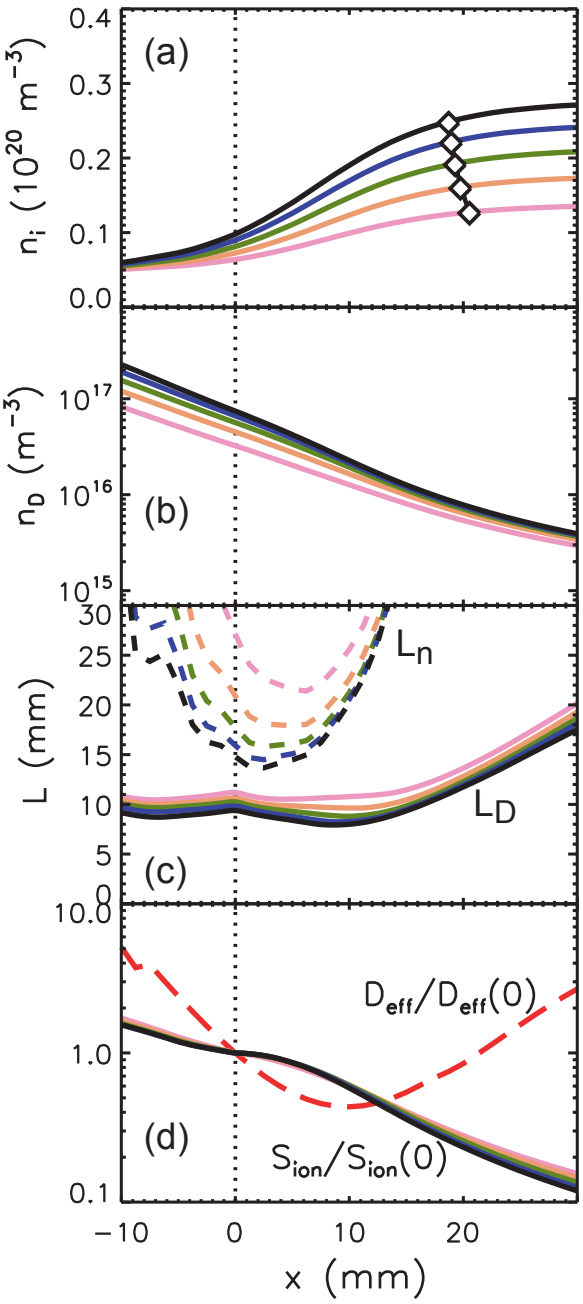

Figure 11: Example profiles from a simulation of fueling perturbation on a modeled low density DIII-D pedestal, ($n_{e,\mathrm{PED}} \approx 2 \times 10^{19}$ m$^{-}3$, $T_{e,\mathrm{PED}} = 600$ eV, $\Delta \approx 20$ mm) using a kinetic treatment for the neutral transport. (a) As in the C-Mod case, computed ion density (n_i) pedestals show an overall rise with neutral source; diamonds demonstrate a trend of pedestal width decreasing with density. (b) Resulting neutral density (n_D) profiles. (c) Local gradient scale lengths of n_i (dashed) and n_D (solid). L_n show much greater variability than in the C-Mod case. (d) Profile shapes for the ionization rate S_{ion} (solid) and the D_{eff} (dashed) used to model the plasma transport.

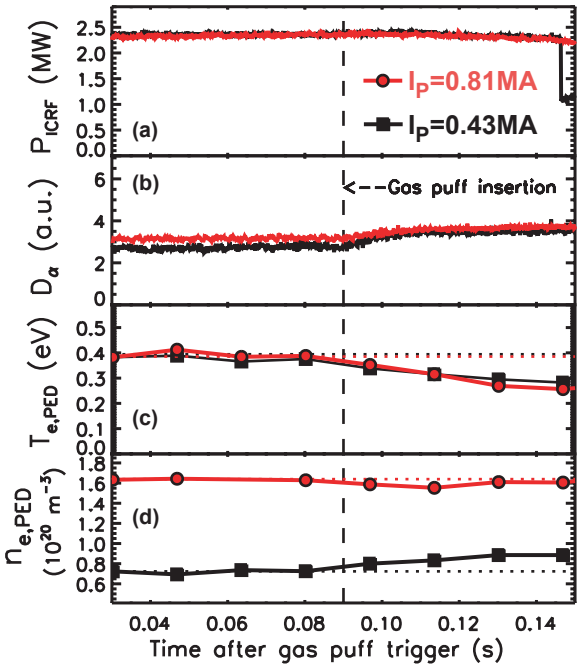

Figure 12: Time evolution of H-modes with agressive D_2 puffing at $I_P = 0.81$, 0.43 MA. (a) Steady ICRF heating is applied during the period studied. (b) Edge D_α shows the time of gas insertion. (c) Subsequent to the D_2 puff, $T_{e,\mathrm{PED}}$ is depressed by nearly 50%. (d) The higher current discharge shows no $n_{e,\mathrm{PED}}$ increase, while an increase at the lower I_P is immediate, leading to a 20% enhancement.

V. DIRECT H-MODE FUELING

Efforts were made to alter the neutral source characteristics in existing H-modes by agressively fueling with D_2 puffs. By increasing the neutral density, presumably the neutral flux at the LCFS is increased, providing the opportunity for both higher core fueling and changes to the density pedestal. A capillary is used to flow D_2 into the H-mode SOL, on the high-field side in most cases. When this supplemental fueling approaches a level of several tens of torr-L/s of gas, a substantial decrease in stored energy and radiated power is exhibited along with a $T_{e,\mathrm{PED}}$ drop of typically 20–30%. Temporal behavior of puffed H-modes is shown in Fig. 12 for two discharges with I_P of 0.81 and 0.43 MA. Constant ICRF power (Fig. 12a) is applied during the H-modes as gas is inserted (vertical dashed line). Figure 12d shows that, in the lower-I_P discharge, the n_e pedestal response is fast and significant. Figure 13 shows that density profiles before and during the D_2 puff have similar gradients and widths, with the puffed profile significantly elevated. There is good qualitative agreement with the results of the neutral perturbation analysis for C-Mod.

Interestingly, the value of $n_{e,\mathrm{PED}}$ in discharges in the standard C-Mod operating range ($I_P \gtrsim$ 0.6 MA) demonstrates relatively little response to excess gas fueling. This is shown by the 0.81 MA trace in Fig. 12d, and also in the time-averaged profiles plotted in Fig. 14. During the puff SOL

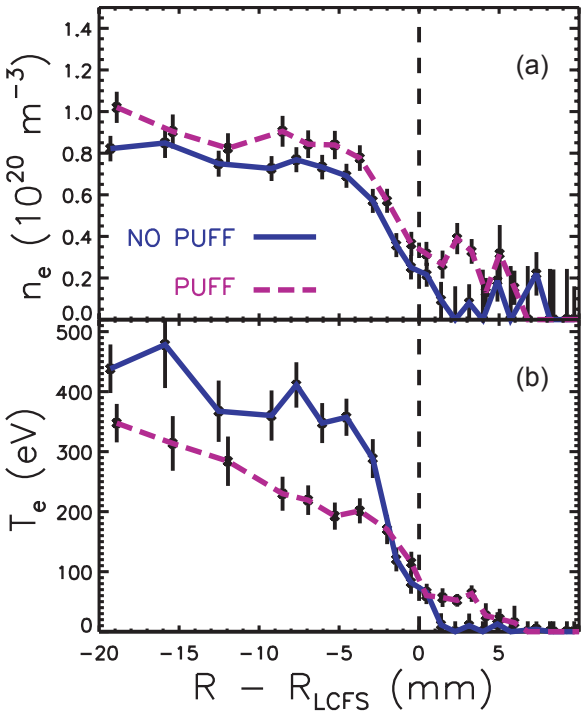

Figure 13: Time-averaged ETS profiles of (a) n_e and (b) T_e in 0.43 MA H-mode before and during D_2 puffing at inner wall. The n_e pedestal becomes elevated by the additional fueling, and $T_{e,\mathrm{PED}}$ is depressed. Characteristic ∇n_e changes little.

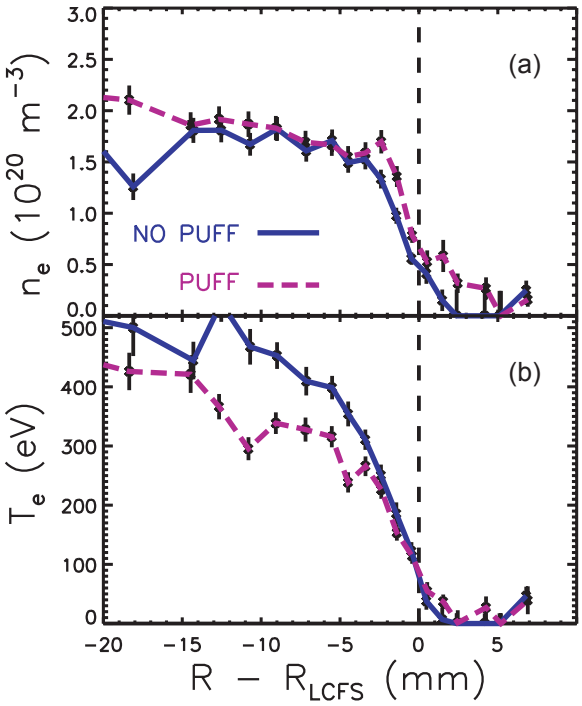

Figure 14: Time-averaged ETS profiles of (a) n_e and (b) T_e in 0.81 MA H-mode before and during D_2 puffing at inner wall. The position of the n_e pedestal shifts outward relative to T_e during the puff. Unlike in the lower-I_P case, the pedestal height stays fixed.

density is seen to rise, and the entire n_e pedestal shifts outward relative to T_e, in a way that is qualitatively consistent with what modeling shows for a neutral source perturbation. Unlike the modeling results, however, $n_{e,\mathrm{PED}}$ does not increase, suggesting that in the case of puffing into a standard H-mode, the pedestal self-screening is higher than predicted, or that plasma transport, assumed fixed in the modeling, is changing in a significant way as the edge parameters change. These results appear to be insensitive to the poloidal location of the gas injection, as several outboard puffs produced the same pedestal behavior. The indication from these data, which are highly reproducible on shots of the same plasma current, are that agressive gas puffing is an ineffective knob for bulk plasma fueling while in high-density H-mode. Opacity of the SOL to neutrals likely plays a key role in this screening. Because the ITER SOL is expected to be similarly opaque, gas fueling may encounter similar difficulties on the future device.

VI. CONCLUSIONS

Improved experimental diagnosis of the ETB region on Alcator C-Mod has yielded substantial insight into the subject of pedestal scalings. Scaling laws determined from steady-state EDA H-modes have demonstrated an I_P^2 limit for the pedestal ∇p_e, which does not appear to be linked to ideal

MHD events or ELMs. In addition, ohmic profiles in the near SOL demonstrate a similar scaling, with the attainable normalized gradient α_{MHD} being determined through the edge collisionality, in a manner that evokes the numerical results of electromagnetic fluid drift turbulence simulations. Scalings of the pressure pedestal with operational parameters are found to be qualitatively consistent with a similar relationship holding in the pedestal. We therefore have evidence that a ballooning-like scaling for edge profiles can be had without ELMs, or even without an H-mode pedestal. Scaling laws also reveal a robust linear dependence of $n_{e,\text{PED}}$ on I_P, with a somewhat weaker scaling with target density in evidence. Under normal C-Mod operation, pedestal widths do not vary significantly with pedestal density, in contrast to a scaling predicted by a simple 1D fluid model for edge neutral penetration.

Particle transport in the pedestal is examined and found to be markedly sensitive to plasma current, increasing as I_P is lowered. This observation, along with the insensitivity of $n_{e,\text{PED}}$ to parameters other than I_P, is strong evidence for plasma transport determining the density pedestal. Much of the enhanced diffusivity at lower current (higher q) is likely due to the formation and increased influence of the QCM in the EDA edge. However, additional drives to plasma transport cannot be ruled out. Because $n_{e,\text{PED}}$ scales linearly with I_P, and is fairly resistant to changes in other parameters, it is difficult to vary significantly the pedestal density without strongly affecting the plasma radial transport. Thus, evaluating the effect of neutral fueling on the pedestal is difficult experimentally. Even agressive gas puffing during H-mode produces only minor effects on the measured density pedestals.

A kinetic treatment of neutral interactions with plasma is used to simulate the effects of fueling on the pedestal. The derived gradient scale lengths, ionization profiles and diffusivity profiles are quite consistent with experimental measurements, and perturbations to the neutral source yield a growth in $n_{e,\text{PED}}$ which agrees well with the empirical scaling with $\bar{n}_{e,L}$. Pedestals more typical of a larger, lower-density machine such as DIII-D are analyzed with the same method. They exhibit greater neutral penetration and show less profile stiffness than in simulations on C-Mod, results qualitatively similar with experimental results as well as predictions from a 1D fluid model for the neutral transport.

The above results suggest that effective modeling of H-mode pedestal profiles requires a coupling of transport models for both the plasma and neutral species. A promising start is made, though further improvements to the work are possible. Additional neutral density data over a wider range of plasma parameters is desired to make more concrete statements about the scaling of transport coefficients, and experimental uncertainties need to be minimized. Poloidal and even toroidal asymmetries in the neutral density need to be further understood, since pedestal formation is a global plasma phenomena, and is unlikely to be governed by the coupling of neutral and plasma transport at one location only. Extension of fueling models to 2D and 3D should occur, employing trusted neutral codes that account for real tokamak geometry and can better account for non-uniformities in wall recycling and other neutral sources. Such work would benefit from

simultaneous measurements of edge neutral emissivity, n_e and T_e at various locations in a given tokamak. Finally, a better physical picture is needed for the processes governing complex plasma transport phenomena, here encapsulated simply as "D_{eff}". In particular, the observed stiffness of pedestal profiles on C-Mod suggests that critical-gradient assumptions may be the appropriate input to pedestal transport models.

ACKNOWLEDGEMENTS

This work was supported by United States Department of Energy Cooperative Agreement Number DE-FC02-99ER54512.

References

[1] M. Greenwald, R. L. Boivin, F. Bombarda *et al.*, Nucl. Fusion **37**, 793 (1997).

[2] C. S. Pitcher, A. H. Boozer, H. Murmann, J. Schweinzer, W. Suttrop and H. Salzmann, Phys. Plasmas **4**, 2577 (1997).

[3] W. Suttrop, M. Kaufmann, H. J. de Blank *et al.*, Plasma Phys. Control. Fusion **39**, 2051 (1997).

[4] T. H. Osborne, R. J. Groebner, L. L. Lao, A. W. Leonard, R. Maingi, R. L. Miller, G. D. Porter, D. M. Thomas and R. E. Waltz, Plasma Phys. Control. Fusion **40**, 845 (1998).

[5] M. Kotschenreuther, W. Dorland, M. A. Beer and G. W. Hammett, Phys. Plasmas **2**, 2381 (1995).

[6] R. E. Waltz, G. M. Staebler, G. W. Hammett and J. A. Konings, Fusion Energy 1996: Proceedings of the 16th International Conference on Fusion Energy, Montreal, 1996 (International Atomic Energy Agency, Vienna, 1997) Vol. 2, p.385.

[7] ASDEX Team, Nucl. Fusion **29**, 1959 (1989).

[8] ITER Physics Expert Group on Confinement and Transport, ITER Physics Expert Group on Confinement Modelling and Database and ITER Physics Basis Editors, Nucl. Fusion **39**, 2175 (1999).

[9] R. J. Groebner and T. H. Osborne, Phys. Plasmas **5**, 1800 (1998).

[10] T. Hatae, Y. Kamada, S. Ishida, T. Fukuda, T. Takizuka, H. Shirai, Y. Koide, M. Kikuchi, H. Yoshida, O. Naito, Plasma Phys. Control. Fusion **40**, 1073 (1998).

[11] G. Saibene, L. D. Horton, R. Sartori *et al.*, Nucl. Fusion **9**, 1133 (1999).

[12] W. Suttrop, O. Gruber, B. Kurzan, H. D. Murmann, J. Neuhauser, J. Schweinzer, J. Stober, W. Treutterer and the ASDEX Upgrade team, Plasma Phys. Control. Fusion **42**, A97 (2000).

[13] T. Onjun, G. Bateman, A. H. Kritz and G. Hammett, Phys. Plasmas **9**, 5018 (2002).

[14] I. H. Hutchinson, R. Boivin, F. Bombarda *et al.*, Phys. Plasmas **1**, 1511 (1994).

[15] R. J. Groebner, T. S. Carlstrom, K. H. Burrell *et al.*, Fusion Energy 1996: Proceedings of the 16th International Conference on Fusion Energy, Montreal, 1996 (International Atomic Energy Agency, Vienna, 1997) Vol. 1, p.867.

[16] Y. Takase, R. L. Boivin, F. Bombarda *et al.*, Phys. Plasmas **4**, 1647 (1997).

[17] M. Greenwald, R. Boivin, P. Bonoli *et al.*, Phys. Plasmas **6**, 1943 (1999).

[18] J. A. Snipes, B. LaBombard, M. Greenwald, I. H. Hutchinson, J. Irby, Y. Lin, A. Mazurenko and M Porkolab, Plasma Phys. Control. Fusion **43**, L23 (2001).

[19] A. Mazurenko, M. Porkolab, D. Mossessian, J. A. Snipes, X. Q. Xu and W. M. Nevins, Phys. Rev. Lett. **89**, 225004 (2002).

[20] H. Zohm, Plasma Phys. Control. Fusion **38**, 105 (1996).

[21] D. A. Mossessian, P. Snyder, A. Hubbard, J. W. Hughes, M. Greenwald, B. LaBombard, J. A. Snipes, S. Wolfe and H. Wilson, Phys. Plasmas **10**, 1720 (2003).

[22] J. W. Hughes, D. A. Mossessian, A. E. Hubbard, B. LaBombard, E. S. Marmar, Phys. Plasmas **9**, 3019 (2002).

[23] A. E. Hubbard, Plasma Phys. Control. Fusion **42**, A15 (2000).

[24] Y. Kamada, R. Yoshino, Y. Neyatani *et al*, Plasma Phys. Control. Fusion **38**, 1387 (1996).

[25] D. A. Mossessian, P. B. Snyder, M. Greenwald, J. W. Hughes, Y. Lin, A. Mazurenko, S. Medvedev, H. R. Wilson and S. Wolfe, Plasma Phys. Control. Fusion **44**, 423 (2002).

[26] O. Sauter, C. Angioni and Y. R. Lin-Liu, Phys. Plasmas **6**, 2834 (1999).

[27] H. R. Wilson, J. W. Connor, A. R. Field, S. J. Fielding, R. J. Hastie, R. L. Miller and J. B. Taylor, Proceedings of the 17th Fusion Energy Conference, Yokahama, 1998 (International Atomic Energy Agency, Vienna, 1998) p.TH3/2.

[28] J. W. Connor, R. J. Hastie, H. R. Wilson and R. L. Miller, Phys. Plasmas **5**, 2687 (1998).

[29] P. B. Snyder, H. R. Wilson, J. R. Ferron, L. L. Lao, A. W. Leonard, T. H. Osborne, A. D. Turnbull, D. Mossessian, M. Murakami and X. Q. Xu, Phys. Plasmas **9**, 2037 (2002).

[30] B. LaBombard, J. A. Goetz, I. Hutchinson *et al*, J. Nucl. Mater. **241–243**, 149 (1997).

[31] B. LaBombard, J. Hughes, M. Greenwald, D. Mossessian and J. L. Terry, Bull. Am. Phys. Soc. **48**, 52 (2003).

[32] B. LaBombard, J. W. Hughes, D. Mossessian, M. Greenwald, B. Lipschultz, J. L. Terry and the Alcator C-Mod Team, Nucl. Fusion **45**, 1658 (2005).

[33] P. N. Guzdar, J. F. Drake, D. McCarthy, A. B. Hassam and C.S. Liu, Phys. Fluids **5**, 3712 (1993).

[34] B. N. Rogers, J. F. Drake and A. Zeiler, Phys. Rev. Lett. **81**, 4396 (1998).

[35] R. J. Groebner, M. A. Mahdavi, A. W. Leonard, T. H. Osborne, N. S. Wolf, G. D. Porter, P. C. Stangeby, N. S. Brooks, R. J. Colchin and L. W. Owen, Nucl. Fusion **44**, 204 (2004).

[36] P. C. Stangeby, J. Phys. D: Appl. Phys. **36**, 2784 (2003).

[37] J. L. Luxon, Nucl. Fusion **42**, 614 (2002).

[38] S. J. Zweben, D. P. Stotler, J. L. Terry *et al.*, Phys. Plasmas **9**, 1981 (2002).

[39] L. C. Johnson and E. Hinnov, J. Quant. Spectrosc. Radiat. Transf. **13**, 333 (1973).

[40] B. LaBombard, M. V. Umansky, R. L. Boivin, J. A. Goetz, J. Hughes, B. Lipschultz, D. Mossessian, C. S. Pitcher, J. L. Terry and the Alcator Group, Nucl. Fusion **40**, 2041 (2000).

[41] Michael Tendler and Daniel Heifetz, Fusion Technol. **11**, 289 (1987).

[42] See EPAPS Document No. _____ for "KN1D: A 1-D Space, 2-D Velocity, Kinetic Transport Algorithm for Atomic and Molecular Hydrogen in an Ionizing Plasma" by Brian LaBombard (2001). This document may be retrieved via the EPAPS homepage (http://www.aip.org/pubservs/epaps.html/) or from ftp.aip.org in the directory /epaps/. See the EPAPS homepage for more information.

[43] Martin Greenwald, Plasma Phys. Control. Fusion **44**, R27 (2002).